University of Reading

Controls on boundary layer ventilation: Boundary layer processes and large-scale dynamics

Article

Published Version

Sinclair, V., Gray, S. L. ORCID: https://orcid.org/0000-0001-8658-362X and Belcher, S. E. (2010) Controls on boundary layer ventilation: Boundary layer processes and large-scale dynamics. Journal of Geophysical Research - Atmospheres, 115. D11107. ISSN 0148-0227 doi: https://doi.org/10.1029/2009JD012169 Available at https://centaur.reading.ac.uk/7652/

It is advisable to refer to the publisher's version if you intend to cite from the work. See Guidance on citing.

To link to this article DOI: http://dx.doi.org/10.1029/2009JD012169

Publisher: American Geophysical Union

All outputs in CentAUR are protected by Intellectual Property Rights law, including copyright law. Copyright and IPR is retained by the creators or other copyright holders. Terms and conditions for use of this material are defined in the End User Agreement.

www.reading.ac.uk/centaur

University of Reading

CentAUR

Central Archive at the University of Reading

Reading's research outputs online

JOURNAL OF GEOPHYSICAL RESEARCH, VOL. 115, D11107, doi:10.1029/2009JD012169, 2010

Click Here for Full Article

Controls on boundary layer ventilation: Boundary layer processes and large-scale dynamics

V. A. Sinclair,[1,2] S. L. Gray,[1] and S. E. Belcher[1]

Received 14 April 2009; revised 8 January 2010; accepted 13 January 2010; published 4 June 2010.

[1] Midlatitude cyclones are important contributors to boundary layer ventilation. However, it is uncertain how efficient such systems are at transporting pollutants out of the boundary layer, and variations between cyclones are unexplained. In this study 15 idealized baroclinic life cycles, with a passive tracer included, are simulated to identify the relative importance of two transport processes: horizontal divergence and convergence within the boundary layer and large-scale advection by the warm conveyor belt. Results show that the amount of ventilation is insensitive to surface drag over a realistic range of values. This indicates that although boundary layer processes are necessary for ventilation they do not control the magnitude of ventilation. A diagnostic for the mass flux out of the boundary layer has been developed to identify the synoptic-scale variables controlling the strength of ascent in the warm conveyor belt. A very high level of correlation (R^2 values exceeding 0.98) is found between the diagnostic and the actual mass flux computed from the simulations. This demonstrates that the large-scale dynamics control the amount of ventilation, and the efficiency of midlatitude cyclones to ventilate the boundary layer can be estimated using the new mass flux diagnostic. We conclude that meteorological analyses, such as ERA-40, are sufficient to quantify boundary layer ventilation by the large-scale dynamics.

Citation: Sinclair, V. A., S. L. Gray, and S. E. Belcher (2010), Controls on boundary layer ventilation: Boundary layer processes and large-scale dynamics, *J. Geophys. Res.*, *115*, D11107, doi:10.1029/2009JD012169.

1. Introduction

[2] The amount of pollution ventilated out of the boundary layer into the free troposphere affects the local air quality and the efficiency of long-range pollution transport. Additionally, the rate that pollutants are transferred into the free troposphere exerts a strong control on the chemistry of the whole atmosphere and can have an impact upon the Earth's radiative forcing.

[3] Midlatitude weather systems have previously been identified to contribute significantly to the ventilation of the boundary layer. Climatologically, *Hess* [2005] showed ascent associated with synoptic weather systems to be the dominant mechanism for ventilating pollutants into the troposphere during winter in the midlatitudes.

[4] Aircraft observations have shown pollutants to be transported long distances in the free troposphere by baroclinic systems [e.g., *Bethan et al.*, 1998; *Bey et al.*, 2001]. Mesoscale modeling studies, with passive tracers included, have been conducted to identify which processes are responsible for boundary layer ventilation during the passage of synoptic systems. *Donnell et al.* [2001] and *Agustí-Panareda et al.* [2005, 2009] partitioned the transport of tracers by transport processes: turbulent mixing within the boundary layer, convection, and large-scale advection. *Donnell et al.* [2001] showed advection by warm conveyor belts associated with frontal systems to be the dominant transport mechanism in three separate case studies. However, results presented by *Agustí-Panareda et al.* [2005] showed that embedded convection within the warm conveyor belt can be as, or more, important than advection for boundary layer ventilation.

[5] Trajectory studies [*Hannan et al.*, 2003; *Eckhardt et al.*, 2004] have shown warm conveyor belts to be an important mechanism by which pollutants can be ventilated into the free troposphere. *Hess and Vukicevic* [2003] investigated pollution transport paths between Asia and North America and found that pollutants are lofted out of the Asian boundary layer in a very narrow band above, and immediately ahead of, the surface cold front before being transported almost isentropically across the Pacific. The transport paths identified by *Hess and Vukicevic* [2003] are in good agreement with conceptual models of airstreams (conveyor belts) within cyclones [e.g., *Harrold*, 1973; *Carlson*, 1980; *Browning*, 1985]. One pollution plume was found to ascend out of the boundary layer and travel anticyclonically away from the surface low, while the second traveled cyclonically around the rear of the low pressure center. Results presented by *Hannan et al.* [2003], who

[1]Department of Meteorology, University of Reading, Reading, UK.
[2]Now at Division of Atmospheric Sciences and Geophysics, Department of Physics, University of Helsinki, Helsinki, Finland.

Copyright 2010 by the American Geophysical Union.
0148-0227/10/2009JD012169

investigated transport from Asia to North America by two different cyclones using in situ and remotely sensed chemical data together with high-resolution meteorological modeling, disagree with the results of *Hess and Vukicevic* [2003]. They showed that the airstreams which transported pollutants into the free troposphere differed considerably from those described in typical conceptual models and were significantly more complex. This disagreement demonstrates the amount of variability between cyclones. *Esler et al.* [2003] emphasized the degree of case-to-case variability in the amount of boundary layer ventilation due to warm conveyor belts by examining two cold front systems over the United Kingdom. They found that the warm conveyor belt associated with the stronger (in terms of minimum surface pressure) of the two systems had an upward mass flux which was 8 times greater than the warm conveyor belt associated with the weaker system.

[6] Previous case studies have attempted to quantify the amount of boundary layer ventilation by calculating the percentage of a tracer, or pollutant, that is transported into the free troposphere. *Kowol-Santen et al.* [2001] found that over a mesoscale model domain 70% of a boundary layer tracer is transported into the free troposphere by a warm conveyor belt in 2 days. Similar values are reported by *Agustí-Panareda et al.* [2005], who found that 68% of a tracer is transported into the free troposphere during the passage of a frontal system, and by *Donnell et al.* [2001], who, in three different case studies, found that between 41% and 52% of the tracer is ventilated out of the boundary layer.

[7] Thus, it is evident that warm conveyor belts are important for boundary layer ventilation. It is also evident that differences exist between the previous case studies. The path that pollutants follow as they are transported out of the boundary layer, and the efficiency of this transport, is not yet fully understood.

[8] In an idealized modeling study *Polvani and Esler* [2007] quantified the amount of boundary layer air uplifted into the troposphere by two inviscid baroclinic life cycles. The two life cycles evolved differently because of differing amounts of barotropic shear in the initial conditions. However, both life cycles ventilated very similar amounts of boundary layer air into the free troposphere. This idealized study was one of the first to attempt to relate the amount of boundary layer ventilation to the characteristics of the cyclone which caused the ventilation. Although *Polvani and Esler* [2007] found the amount of ventilation to be insensitive to barotropic shear, they hypothesized that the amount of ventilation is largely controlled by the amplitude of the baroclinic wave and hence the vertical velocity of the growing wave.

[9] *Sinclair et al.* [2008] expanded the work of *Polvani and Esler* [2007] by simulating the same two life cycles, but in the presence of a boundary layer parameterization scheme, and found that the inclusion of boundary layer processes increased the overall amount of ventilation while retaining the similarity between the two life cycles. *Sinclair et al.* [2008] also identified three interlinked processes that were responsible for the redistribution of tracers within both the boundary layer and the free troposphere during the evolution of the two contrasting dry baroclinic life cycles. (Transport by moist convection was excluded in their experiments.) Tracer was found to be transported vertically within the boundary layer by turbulent mixing, horizontally within the boundary layer by convergence and divergence induced by surface friction and the large-scale dynamics, and into and through the free troposphere by large-scale advection associated with the warm conveyor belt. *Sinclair et al.* [2008] hypothesized that the ascent associated with the warm conveyor belt is one control on the amount of boundary layer ventilation but also noted how important the boundary layer transport processes were in the overall ventilation process. Specifically, it was identified that the horizontal transport by convergence and divergence within the boundary layer may act to enhance the amount of ventilation by increasing the rate at which tracer is supplied to the source region of the warm conveyor belt.

[10] Therefore, in this paper, experiments are described that have been designed to test the relative importance of the two transport processes highlighted by *Sinclair et al.* [2008] and to identify which process acts as the limiting step in the total amount of boundary layer ventilation. These experiments also allow the theoretical statement of *Polvani and Esler* [2007], that the large-scale vertical velocity in the life cycle determines the amount of ventilation, to be rigorously tested. This is achieved by simulating a variety of carefully selected baroclinic life cycles using an idealized version of the Met Office Unified Model. A passive tracer is included to represent pollutants.

[11] The structure of this paper is as follows. Section 2 describes the numerical model used for these simulations and the initial conditions (dynamical and tracer) of the life cycle experiments. The evolution of the control baroclinic life cycle is described in section 3. Section 4 describes the range of experiments conducted and the motivation for selecting these experiments. The importance of the horizontal transport within the boundary layer is investigated in section 5, and the ventilation dependence on the large-scale dynamics is presented in section 6. Conclusions are then presented in section 7.

2. Numerical Model and Initial Conditions

2.1. Idealized Met Office Unified Model

[12] The baroclinic life cycles are all simulated using the Met Office Unified Model (MetUM), version 6.1, which solves the full primitive equations and is nonhydrostatic. The MetUM is used in idealized mode and is configured into a channel model with east-west periodic boundary conditions and fixed north-south lateral boundaries. The horizontal grid spacing is 0.4° in both longitude and latitude, which corresponds to an approximate grid spacing of 44.5 km. The vertical configuration consists of 38 nonuniformly distributed levels, with the highest resolution in the boundary layer (level spacing of ~100 m decreasing to ~800 m in the upper troposphere). The full dynamics from the global operational model, as described by *Davies et al.* [2005], are applied in the idealized configuration. Two differences do exist between the operational MetUM and this idealized version. First, a cartesian coordinate system is used in the idealized model instead of the standard spherical polar coordinates that are used operationally. Second, a f plane approximation is used in the idealized version rather than $f = 2\Omega \sin \phi$, which is used operationally.

[13] The simulations presented in this paper are performed without the radiation parametrization scheme acting, with no diurnal cycle, with no orography, and with no moisture present. The only physical parametrization that is applied is the complete version of the standard MetUM boundary layer scheme, which is used in all simulations. The boundary layer scheme calculates surface fluxes using bulk aerodynamic formula, with Monin-Obukhov similarity theory applied to calculate the stability corrections to the neutral drag coefficients. Above the surface layer, both local and nonlocal mixing is parametrized. K theory is used to calculate fluxes resulting from local mixing, and nonlocal mixing is parametrized through nonlocally determined eddy diffusivity profiles. Further details can be found in the work of *Lock et al.* [2000].

[14] The boundary layer depth is diagnosed off-line using a parcel ascent method, similar to that described by *Troen and Mahrt* [1986]. The bulk Richardson number, Ri_b, is calculated between the surface and subsequent higher levels in the model using

$$Ri_b z = \frac{\frac{g}{\theta_s}(\theta z - \theta_{s'})z}{uz^2 + vz^2}, \tag{1}$$

where z denotes the height of the model level at which the Richardson number is evaluated, θ is potential temperature, and u and v are the horizontal velocity components. The variable $\theta_{s'}$ is an appropriate temperature of air near the surface, estimated by

$$\begin{aligned} \theta_{s'} &= \theta_1 + b\frac{\overline{(w'\theta')}_0}{(u*/\phi_m)} \quad \text{if} \quad \overline{(w'\theta')}_0 > 0 \\ \theta_{s'} &= \theta_1 \qquad\qquad\qquad\quad \text{if} \quad \overline{(w'\theta')}_0 \le 0, \end{aligned} \tag{2}$$

where θ_1 is the potential temperature at the lowest mode level, $\overline{(w'\theta')}_0$ is the virtual surface heat flux, and ϕ_m is the dimensionless vertical wind gradient for unstable conditions. The variable b is a dimensionless constant taken to be 8.5 as given by *Holtslag and Boville* [1993]. The boundary layer depth is diagnosed to be at the level where the bulk Richardson number exceeds a critical value (0.25). If this level lies between model levels, a linear interpolation is performed between the level where the Richardson number exceeds the critical value and the level below.

2.2. Model and Tracer Initialization

[15] Baroclinic life cycles are initiated by specifying a typical wintertime storm track situation, a strong westerly upper level jet and associated north-south temperature gradient, and then adding a small temperature perturbation to this background state. The baroclinic life cycles that are simulated here are initialized using a very similar method to that described by *Polvani and Esler* [2007]. The background state consists of a zonal wind profile that is a function of latitude (ϕ) and height (z):

$$u(\phi, z) = U_0 F(\phi)\left[\frac{z}{z_t}\exp\left(-\frac{(z/z_t)^2 - 1}{2}\right)\right]. \tag{3}$$

U_o is the maximum strength of the upper level jet, taken to be 45 m s^{-1} in the control simulation, and z_t is the tropopause height, taken to be 13 km. $F(\phi)$ is a latitudinal dependence given by

$$F(\phi) = \{\sin[\pi(\sin\phi)^2]\}^3. \tag{4}$$

During the initialization the meridional wind component is set to 0. A reference potential temperature profile (located in the center of the domain) is defined by

$$\begin{aligned} \theta(z) &= \theta_{\text{ref}} + z\left(\frac{\partial\theta}{\partial z}\right)_{\text{trop}} \qquad \text{if} \quad z \le z_t \\ \theta(z) &= \theta_{z_t} + (z - z_t)\left(\frac{\partial\theta}{\partial z}\right)_{\text{strat}} \qquad \text{if} \quad z > z_t, \end{aligned} \tag{5}$$

where θ_{ref} is the surface potential temperature (280 K), θ_{zt} is the potential temperature at height z_t, and z is the height above ground. Within this reference profile two layers are specified, one that is representative of the troposphere ($(\partial\theta/\partial z)_{\text{trop}}$) and one that is representative of the stratosphere ($(\partial\theta/\partial z)_{\text{strat}}$). In the control experiment the lower, tropospheric layer has a constant potential temperature gradient of 0.004 K m^{-1} that extends from the surface to 13 km (z_t). The second, stratospheric layer (above 13 km) has a stronger stratification; the potential temperature gradient is 0.016 K m^{-1}. This value was chosen as *Rotunno and Bao* [1996] recommend that the stratification of the stratosphere is four times that of the troposphere. The full potential temperature field, which is independent of longitude, is then calculated by integrating thermal wind balance with the prescribed wind fields and the reference potential temperature profile.

[16] The surface temperatures are set equal to the lowest model level temperatures at the initial time and are then held constant throughout the simulations. A balanced pressure field is found by integrating the hydrostatic balance equation. The height-independent temperature perturbation (T') that is added to this baroclinically unstable jet has the form

$$T'(\lambda, \phi) = \widehat{T}\cos(m\lambda)\{\text{sech}[m(\phi - \widehat{\phi})]\}, \tag{6}$$

where m is the zonal wave number, taken to be 6 in all experiments, λ is longitude, and $\widehat{\phi}$ is the latitude that the jet is centered upon (45°N in the control experiment). $\widehat{T}$ is the maximum temperature perturbation, which equals 1 K in all experiments.

[17] A passive tracer is included in these simulations to represent pollutants emitted within the surface layer. The tracer is acted upon by the large-scale winds and turbulent motions as diagnosed by the boundary layer scheme. A constant uniform source of tracer is included in all simulations and is located at the lowest model level. In the initial conditions the tracer concentration is set to zero throughout the whole domain. Tracer is emitted uniformly across the domain at a rate of 1×10^{-4} kg m^{-2} s^{-1}, and there are no sinks present. The exact magnitude of the source is unimportant as it can be shown by considering the tracer equation in flux form that the resulting tracer concentrations throughout the whole domain are directly proportional to the source strength. The tracer is advected by the standard semi-Lagrangian advection scheme that is used to advect

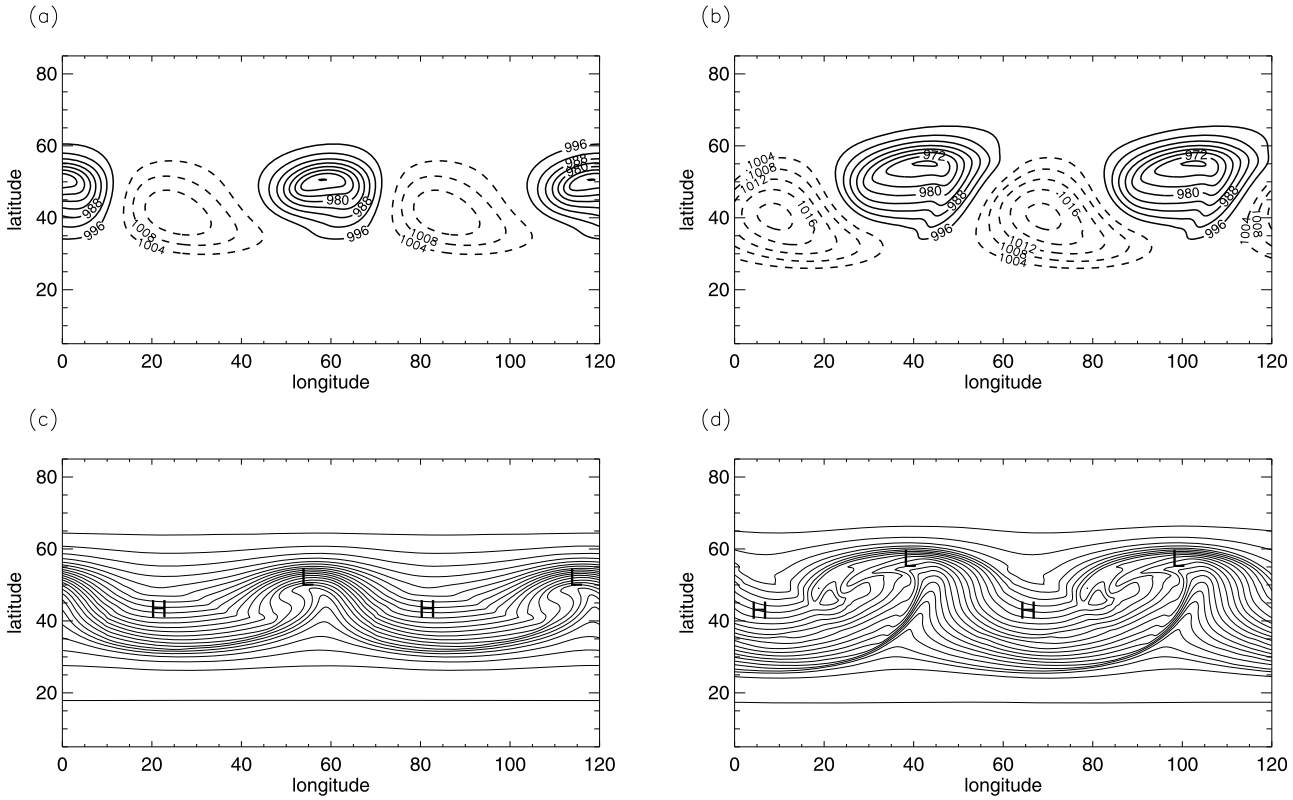

Figure 1. Surface pressure after (a) 8 days and (b) 12 days. Pressure contours are drawn every 4 h Pa with the 1000 h Pa contour omitted. Solid black contours show values less than 1000 h Pa, and dashed contours show values greater than 1000 h Pa. Potential temperature (contour interval 2 K) at 980 m after (c) 8 days and (d) 12 days. L marks the minimum pressure and H the maximum. Note that two domains are plotted next to each other here and in Figure 3.

dynamical variables in the operational MetUM, except that a flux redistribution method [*Roe*, 1986] is applied to ensure that negative tracer values do not appear.

3. Description of the Control Life Cycle

[18] Figures 1a and 1b show the surface pressure pattern in the control life cycle after 8 and 12 days, respectively. By day 8 features resembling typical cyclones and anticyclones are evident. However, at this stage there is little meridional displacement of the cyclones and anticyclones, and from the pressure contours alone no fronts can be identified. When the near-surface potential temperature distribution after 8 days is considered (Figure 1c), a warm front to the north of the low center and a weak cold front to the southwest of the low center can be identified. After a further 4 days of development the system has reached its mature stage; the minimum pressure is now 966 h Pa. The surface pressure (Figure 1b) shows that the low center has moved poleward; it is now located at 55°N, compared to 50°N 4 days previously. Additionally, there is now a pressure trough evident on the western edge of the warm sector which marks the location of the cold front. Figure 1d shows that by day 12 the cold front has intensified considerably and now has a large meridional extent, reaching from 30°N to 55°N. Additionally, by day 12 a portion of the warm front has been advected around the low center by strong easterly winds to form a bent-back warm front [*Shapiro and Keyser*, 1990].

4. Experimental Design

[19] Two sets of experiments are conducted. The first set is designed to investigate the effect of the horizontal transport within the boundary layer on the amount of boundary layer ventilation, and the second is designed to investigate the effect of the large-scale dynamics on the amount of boundary layer ventilation. Two possible ventilation regimes exist. In the first possible regime transport by the horizontal divergence and convergence within the boundary layer acts as the limiting factor in the amount of ventilation. In this regime the flux of tracer out of the boundary layer by the warm conveyor belt exceeds the flux into the boundary layer source regions of the warm conveyor belt by convergence. Consequently, the warm conveyor belt source region becomes depleted of tracer, and the full ventilation potential of the cyclone is not fulfilled. The second possible regime is the direct opposite; the strength of the warm conveyor belt acts as the constraint on the amount of ventilation. In this regime the flux of tracer into the source region of the boundary layer exceeds the flux out of the boundary layer by

Table 1. Values of the Surface Drag Coefficient Used

Drag Coefficient	Type of Surface	Name
0	unphysical	no drag
0.1×10^{-3}	ice	smooth
0.56×10^{-3}	water	ocean drag
2.0×10^{-3}	smooth land (plains, farmland)	land drag
5.0×10^{-3}	rough land (forests, urban)	rough land drag

the warm conveyor belt, and thus, there will always be adequate amounts of tracer available in the source region of the warm conveyor belt for venting. The experiments conducted here aim to identify which regime exists in typical midlatitude weather systems.

4.1. Experiments on Boundary Layer Control on Ventilation

[20] Surface friction has two well-documented effects on cyclones. First, friction acts to spin down cyclones, resulting in slower development, weaker systems, and, hence, weaker vertical velocities [*Williams and Robinson*, 1974; *Simmons and Hoskins*, 1978; *Farrell*, 1985; *Adamson et al.*, 2006]. Second, friction acts to deflect winds away from the geostrophic direction. In cyclonic regions this results in enhanced convergence, and hence by mass conservation, vertical motion out of the boundary layer. This vertical motion is referred to as Ekman pumping [*Ekman*, 1905]. As friction increases, the wind turns farther away from the geostrophic direction, increasing the amount of convergence within cyclonic regions of the boundary layer [*Holton*, 1992]. Therefore, the importance of the horizontal transport of tracer within the boundary layer is investigated here by modeling baroclinic life cycles with differing levels of surface friction. Numerically, this is achieved by changing the value of the surface drag coefficient, C_d. In the control experiment, described in section 3, the drag coefficient varies spatially and temporally as the boundary layer scheme calculates the drag coefficient as a function of stability at each individual grid point. However, in the sensitivity experiments the drag coefficient was held fixed in time and uniform across the domain.

[21] Five baroclinic life cycles with different drag coefficients have been simulated; the drag coefficient values are presented in Table 1. The only difference between these five experiments and the control experiment is the value of the surface drag coefficient. Three of the five drag coefficient values ($C_d = 0$, $C_d = 0.56 \times 10^{-3}$, and $C_d = 2.0 \times 10^{-3}$) were selected to be the same as values used in a previous study by *Hines and Mechoso* [1993], who investigated the influence of surface drag on frontal structure. This allows the dynamical response of the fronts to the presence of drag in the idealized MetUM to be compared directly to the results of *Hines and Mechoso* [1993]. The smooth drag ($C_d = 0.1 \times 10^{-3}$) experiment was included to help relate the results of the no drag experiment to the others; without this additional experiment there is a large range of unexplored parameter space. The rough land experiment was included as it is suggested by *Stull* [1988] that values of C_d vary between 1×10^{-3} and 5×10^{-3}, and *Arya* [1999] notes that, over land, values of C_d can vary between 0 and 1×10^{-2}.

4.2. Experiments on Large-Scale Control on Ventilation

[22] First, we identify the parameters that control the magnitude of large-scale ascent and hence the amount of boundary layer ventilation. Applying typical scaling arguments [*Haltiner and Williams*, 1980] to the omega equation, or by examination of the Eady model [*Hoskins et al.*, 2003], the vertical motion in baroclinic life cycles can be shown to scale as

$$w \sim \frac{V_g f_0 (\partial U_g / \partial z)}{2N^2}, \tag{7}$$

where w is vertical velocity (in m s^{-1}), V_g is the geostrophic wind velocity, f_0 is the Coriolis parameter, $\partial U_g/\partial z$ is the vertical wind shear, and N is the Brunt-Väisälä frequency. Numerical experiments have been designed and conducted to test the dependence of boundary layer ventilation on the values of $\partial U_g/\partial z$, N, and f_0.

[23] The magnitude of the vertical shear is altered by varying the maximum strength of the zonal jet in the initial conditions (U_0 in equation (3)) while keeping the height of the jet constant at 13 km. Five different values of the maximum jet strength were used: 35, 40, 45 (the control life cycle), 50, and 55 m s^{-1}. Four values of tropospheric stability ($(\partial\theta/\partial z)_{\text{trop}}$ in equation (5)) were investigated: the value in the control run, 0.004 K m^{-1}; a slightly more stable value, 0.006 K m^{-1}; a very stable value, 0.008 K m^{-1}; and a less stable value, 0.003 K m^{-1}. In the stratosphere the initial value of $(\partial\theta/\partial z)_{\text{strat}}$ was kept constant in all experiments. Life cycles with zonal jets centered on four different latitudes ($\widehat{\phi}$ in equation (6)) were simulated: 40°N, 45°N (the control latitude), 50°N, and 55°N. The value of the Coriolis parameter also varied in these four experiments and was calculated by $f_0 = 2\ \Omega \sin \widehat{\phi}$, where Ω is the rotation rate of the Earth.

5. Dependence of Ventilation on Boundary Layer Transport Processes

5.1. Effect of Surface Drag on Life Cycle Dynamics and Mass and Tracer Fluxes

[24] Figure 2 shows that increasing the surface drag coefficient decreases the growth rate, and reduces the eddy kinetic energy, of the life cycles. The frontal structures also change with increasing surface drag. Figure 3 shows the potential temperature at 980 m for three of the five life cycles with different surface drag coefficients. To ensure a fair comparison, the frontal structures are compared when each of the cyclones has a similar intensity, diagnosed by both minimum central pressure and eddy kinetic energy (see Table 2).

[25] In the no drag case (Figure 3a) there is a very strong warm front to the northeast of the low pressure center and a weak cold front to the southwest of the low center. In the ocean drag experiment (Figure 3c) the warm front is strong but more diffuse than in the no drag experiment, and the cold front is of comparable intensity to the cold front in the no drag case. In the rough land experiment (Figure 3e) the warm front is weak and diffuse, but the cold front is slightly stronger than in the ocean drag experiment.

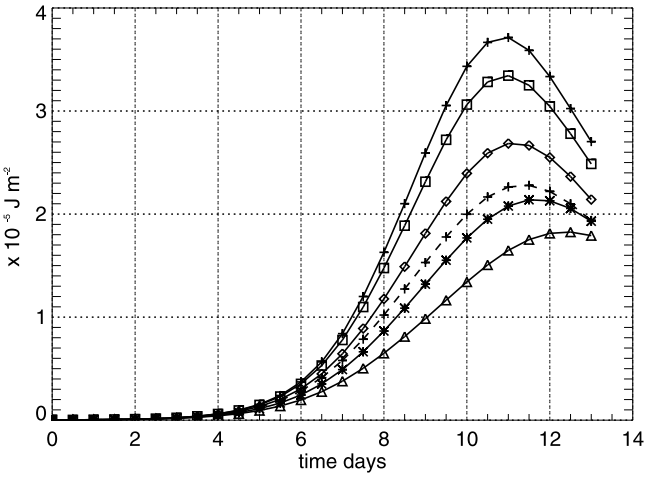

Figure 2. Domain-averaged eddy kinetic energy. Crosses, no drag; squares, smooth drag; diamonds, ocean drag; asterisks, land drag; and triangles, rough land drag. Dashed line with crosses indicates the control life cycle.

[26] These dynamical results agree with the results of *Hines and Mechoso* [1993], who found warm fronts to be more sensitive to the amount of surface drag than cold fronts. Figures 3a, 3c, and 3e also demonstrate that life cycles which resemble real midlatitude cyclones have been successfully simulated here for a range of surface drag coefficients.

[27] Figure 3 also shows the spatial distribution of the mass flux between the boundary layer and free troposphere. In the no drag experiment (Figure 3b) mass is only ventilated out of the boundary layer in the warm front region. There is ventilation in this region as the warm conveyor belt is forced to rise up and over the warm frontal zone and the cool air ahead of the warm front. Tracer (not shown) is also only fluxed out of the boundary layer in the warm front location.

[28] In the ocean drag experiment (Figure 3d) the boundary layer is ventilated in two locations. First, in the warm front region, as was the case in the no drag experiment, and second, ahead of the cold front. The ventilation ahead of the cold front is due to a narrow band of convergence-driven ascent that the warm conveyor belt experiences. Tracer (not shown) is fluxed out of the boundary layer in the same two regions as mass. In the rough land experiment (Figure 3f) there are large mass fluxes ahead of the cold front, again which are due to the warm conveyor belt.

[29] Therefore, it can be concluded that the warm conveyor belt is the physical process leading to ventilation and that the location of the ventilation changes with increasing surface drag from the warm front region to the cold front region. This is in agreement with the dynamical changes (potential temperature gradients) that the fronts experience with surface drag.

5.2. Effect of Surface Drag on Total Amount of Mass and Tracer Ventilation

[30] Figure 4a shows the mass flux out of the boundary layer integrated over the whole domain as a function of time for all experiments with different drag coefficients. This is calculated by

$$F_M = \int_A \rho w_h dA, \tag{8}$$

where F_M is the domain-integrated mass flux, A is the area where $w_h > 0$, ρ is the density of air, and w_h is the vertical velocity interpolated onto the surface identified as the boundary layer top. The most notable result is that the domain-integrated mass flux (the rate that mass is ventilated out of the boundary layer) is insensitive to the value of the drag coefficient.

[31] The domain-integrated tracer flux, F_T, (Figure 4b) is calculated by

$$F_T = \int_A \rho C_h w_h dA, \tag{9}$$

where C_h is the tracer concentration on the boundary layer top. For all experiments the rates of tracer ventilation are very similar to each other for the first 9 days. After this time, the tracer flux in both the no drag and smooth drag experiments increases more slowly and is smaller than the mass flux. This suggests that tracer is not available in adequate concentrations in the region of the boundary layer that is ventilated by large-scale ascent, presumably because tracer is ventilated out of the boundary layer more quickly than it is concentrated by boundary layer convergence. This hypothesis will be tested in section 5.3.

[32] Figure 5 shows the total amount of mass and tracer transported out of the boundary layer over the whole domain and throughout the life cycle (days 0–13) for all experiments with different drag coefficients. The amount of mass transported out of the boundary layer is remarkably insensitive to surface drag; there is a 15% increase in the mass flux between the smooth drag experiment and the rough land experiment (a factor of 50 difference in the drag coefficient). The tracer flux is more sensitive to surface drag than the mass flux when low values of drag are considered. However, the tracer flux is also found to be largely unaffected by surface drag once larger values are considered; there is almost no change in the tracer flux between the land and rough land case despite the drag coefficient more than doubling.

[33] To summarize, it can be concluded that the presence of friction acts like an "on-off" switch. With low (somewhat unrealistic) levels of surface friction the ventilation of tracer is reduced. However, once a certain threshold in the amount of friction has been reached, for example, the value used in the ocean experiment, 0.56×10^{-3}, further increases in friction do not increase the amount of tracer ventilated out of the boundary layer.

5.3. Boundary Layer Tracer Budgets

[34] The purpose of this section is to explain the decrease in tracer ventilation in the no drag and smooth drag experiments. It is hypothesized that this occurs because with little surface drag there is minimal friction-induced divergence out of the anticyclone or convergence into the cyclonic source region of the warm conveyor belt. Therefore, with limited friction acting, the tracer will not be

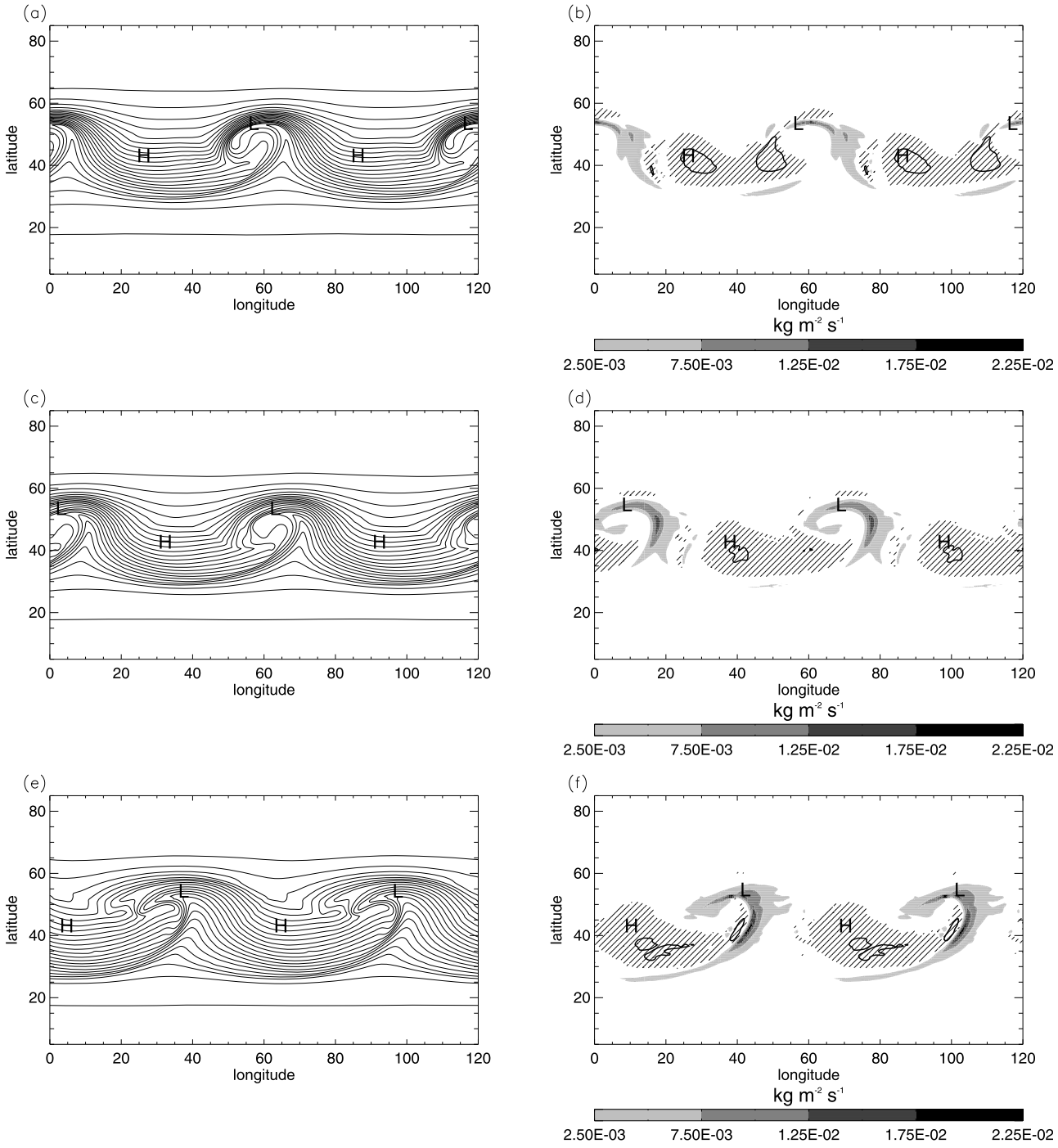

Figure 3. (left) Potential temperature at 980 m and (right) mass flux out of the boundary layer at the times given in Table 2. (a, b) No drag, (c, d) ocean drag, and (e, f) rough land drag. L marks the location of the minimum pressure, and H marks the location of the maximum pressure. In Figures 3b, 3d, and 3f positive values indicate a flux from the boundary layer to the free troposphere and negative values indicate a flux from the free troposphere to the boundary layer. Hatching shows mass fluxes which are less than -2.5×10^{-3} kg m^{-2} s^{-1}. The thick black contour is the -1.0×10^{-2} kg m^{-2} s^{-1} contour.

transported within the boundary layer to the source regions of the conveyor belt as efficiently as in the experiments with large amounts of surface friction.

[35] To quantify how tracer is lost and gained from the boundary layer source region of the warm conveyor belt, individual terms in a tracer budget equation are evaluated. The tracer budget equation, which is closely related to the mass budget equation derived by *Sinclair et al.* [2009], can be written as

$$\frac{\partial \widehat{\rho_t}}{\partial t} = (\rho_t)_h \frac{\partial h}{\partial t} - \widehat{D}_t + A_t + S - \overline{(w'\rho_t')}_h, \qquad (10)$$

Table 2. Time That Potential Temperature and the Mass Flux Are Plotted at in Figure 3 and Minimum Pressure at That Time

Experiment	Day	Minimum Pressure (hPa)
No drag	8.0	958
Ocean drag	9.0	963
Rough land	12.0	967

where a circumflex represents a quantity integrated over the depth of the boundary layer (e.g., $\widehat{x} = \int_0^h x dz$). The variable ρ_t is the density of tracer, (given by tracer concentration, C, multiplied by the density of air, ρ), h is the boundary layer depth, and a subscript h indicates quantities on the boundary layer top. S is the surface source of tracer, and $(\overline{w'\rho_t'})_h$ is the turbulent flux of tracer across the boundary layer top. The expression $(\rho_t)_h(\partial h/\partial t)$ represents the rate of change of tracer mass within the boundary layer due to changes in boundary layer depth. $\widehat{D}_t$ is the boundary layer depth integrated divergence of tracer given by

$$\widehat{D}_t = \frac{\partial}{\partial x}(\widehat{u\rho_t}) + \frac{\partial}{\partial y}(\widehat{v\rho_t}), \tag{11}$$

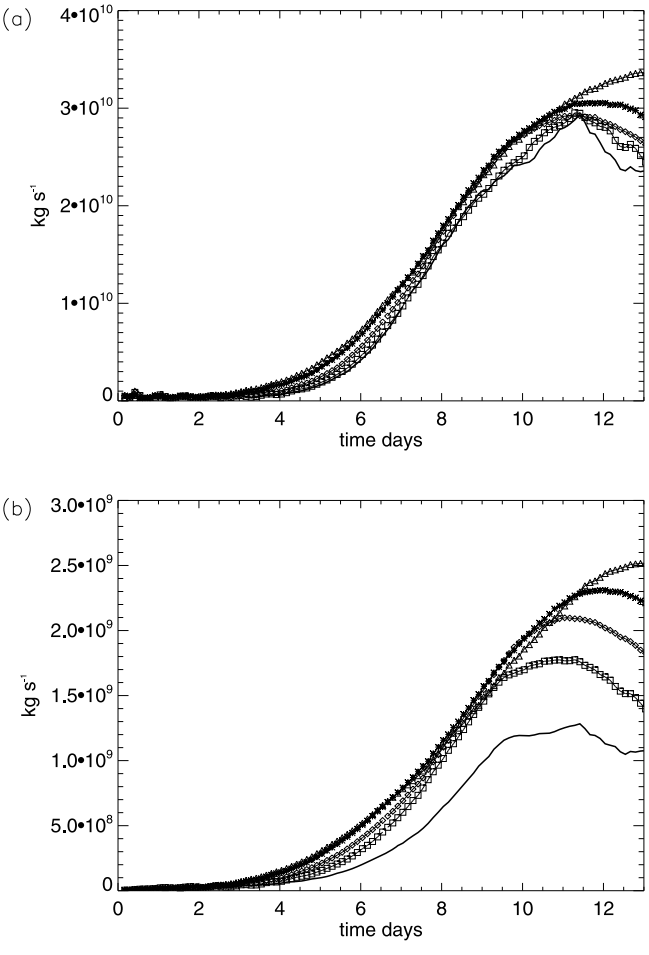

Figure 4. (a) Domain-integrated mass flux out of the boundary layer and (b) domain-integrated tracer flux out of the boundary layer. Solid line (no markers), no drag; squares, smooth drag; diamonds, ocean drag; asterisks, land drag; and triangles, rough land drag.

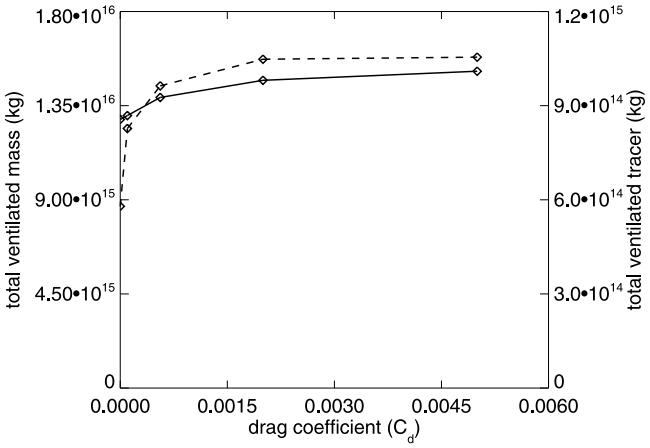

Figure 5. Total mass of air (solid line) and total mass of tracer (dashed line) ventilated out of the boundary layer during the whole life cycle.

and A_t is large-scale advection of tracer given by

$$A_t = (u\rho_t)_h \frac{\partial h}{\partial x} + (v\rho_t)_h \frac{\partial h}{\partial y} - (\rho_t w)_h, \tag{12}$$

where u, v, and w are the three wind components.

[36] To quantify the balance between the convergence term and the large-scale advection term, the rate of change of boundary layer tracer mass due to each of these two processes is integrated over the area identified as the warm conveyor belt footprint. This is defined as the area enclosed within the 0.65 cm s^{-1} vertical velocity contour on the boundary layer top. This specific value was selected to be consistent with the definition used by *Sinclair et al.* [2008]. The same has also been done for the source term and the turbulent flux term as these two additional processes can alter the amount of tracer available in the footprint region. The $(\rho_t)_h(\partial h/\partial t)$ term is not considered as it causes very small changes to the boundary layer integrated tracer mass. This is because, as the boundary layer depth decreases [increases], the tracer within the boundary layer remains trapped within the boundary, causing the tracer concentrations to increase [decrease], but the total mass of tracer remains the same. However, it should be noted that if a mass budget was considered, rather than a tracer budget, then this term would be significant.

[37] Figure 6 shows the rate of change of tracer mass, integrated over the conveyor belt footprint region, due to these four processes for the smooth drag and rough land drag experiments. The large-scale advection and convergence within the boundary layer are the dominant terms. The surface emission and turbulent flux terms are both small.

[38] In the smooth drag experiment (Figure 6a) the increase of tracer mass due to convergence is greater than the decrease in tracer mass due to the large-scale vertical motion up until day 10. After this point, the tracer convergence is weaker than the removal of tracer due to vertical motion, and hence, there is not sufficient tracer in the warm conveyor belt source region to realize the full ventilation potential of the life cycle. In the rough land experiment

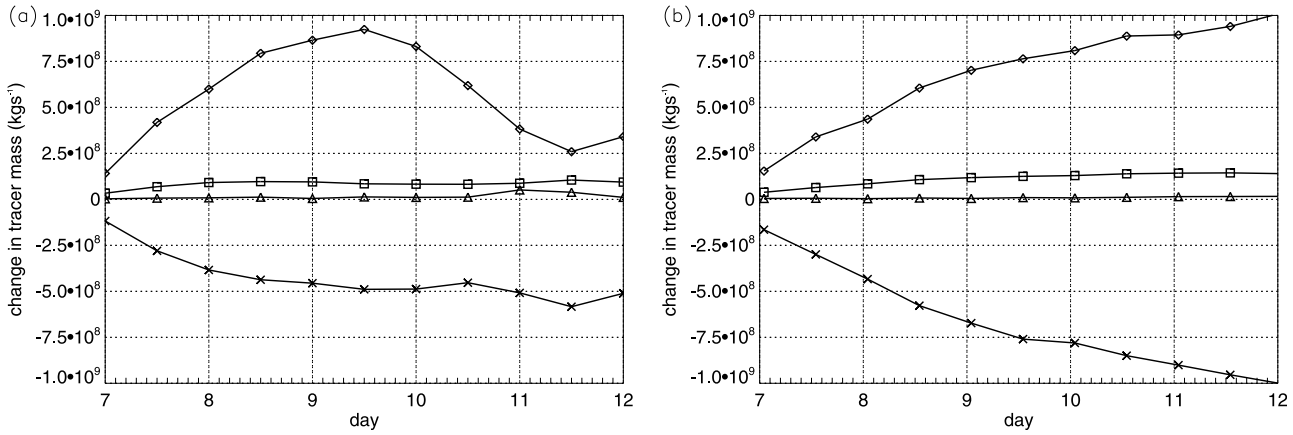

Figure 6. Rate of change of tracer mass (evaluated over 30 min) in the boundary layer within the conveyor belt source region as a function of time due to horizontal convergence (diamonds), large-scale advection (crosses), surface emission of tracer (squares), and turbulent exchange between the boundary layer and free troposphere (triangles). (a) Smooth drag experiment and (b) rough land drag experiment.

(Figure 6b) the supply of tracer mass due to convergence appears well balanced with the removal of tracer by large-scale advection at all times.

[39] This indicates that the hypothesis stated previously, that with little frictionally induced convergence tracer is not supplied into the conveyor belt footprint rapidly enough, is only true during the latter stages of the smooth drag experiment. This demonstrates that the two hypothesized regimes both exist. However, the regime in which boundary layer transport by divergence and convergence acts as the limiting step only occurs for unrealistically small values of surface drag. This evidence, combined with the mass flux's lack of sensitivity to surface drag, allows us to conclude that the boundary layer transport processes do not control the amount of boundary layer ventilation.

6. Dependence of Ventilation on Large-Scale Dynamics

[40] We now turn to the role of the large-scale dynamics in controlling boundary layer ventilation. Figure 7 shows the mass and tracer fluxes for experiments with different jet strengths, tropospheric stabilities, and jet center latitudes. It is evident from Figure 7a that as the maximum jet speed increases, the mass flux out of the boundary layer increases. Therefore, cyclones that develop in association with a stronger midlatitude jet will be more efficient at ventilating the boundary layer. Similar behavior is observed for the tracer flux (Figure 7b); the maximum value of tracer flux increases with increasing jet strength. Figures 7c and 7d show the variation of the mass and tracer flux with varying tropospheric stability. The rate of ventilation of both mass and tracer is found to increase significantly with decreasing tropospheric stratification. Figures 7e and 7f show the effect of the latitude of the jet's center (and hence the value of the Coriolis parameter) on the mass and tracer fluxes. Larger mass and tracer fluxes are found for life cycles which have their zonal jets located more northerly and hence have larger Coriolis parameters. However, the effect of latitude on the amount of ventilation is weaker than either the effect of the jet's strength or the troposphere's stratification.

6.1. A Combined Diagnostic for Boundary Layer Ventilation

[41] In this section a diagnostic for the warm conveyor belt mass flux is derived. The mass flux is given by

$$MF = w_{\mathrm{wcb}} A_{\mathrm{wcb}} \rho, \tag{13}$$

where w_{wcb} is the vertical velocity in the warm conveyor belt, A_{wcb} is the area that the ascent occurs over, and ρ is density, which, for simplicity, is assumed to have a constant value of 1 kg m^{-3}. Vertical velocity is estimated using equation 7. All variables in equation (7) are estimated from those specified in the initial conditions. Therefore, V_g is approximated using the only velocity scale present: the maximum jet speed (U_0). The vertical shear is estimated using U_0/H, where H is the height of the jet. The Coriolis parameter, f_0, is specified in the initial conditions and is calculated using the latitude that the zonal jet is centered on. The Brunt-Väisälä frequency, N, is calculated from the reference potential temperature profile, again which is specified in the initial conditions. The area, A_{wcb}, is defined as a length scale, L, squared. The length scale is found by calculating the wavelength of the baroclinic systems; $\lambda = 2\pi a/m$, where a is the Earth's radius and m is the wave number. The length scale is then estimated from $L = \lambda/4$, yielding $A_{\mathrm{wcb}} = (\pi a/2m)^2$. Substituting A_{wcb} and equation (7) into equation (13) allows the mass flux of a given baroclinic system to be estimated by

$$MF = \rho \left(\frac{\pi a}{2m}\right)^2 \frac{U_0 f_0 \left(U_{jet}/H\right)}{2N^2}. \tag{14}$$

This mass flux diagnostic can be tested by plotting the actual amount of ventilation against this diagnostic. Figure 8a shows the maximum domain-integrated rate of ventilation of mass that occurs during the whole life cycle for the 11 different experiments varying large-scale parameters plotted against the diagnostic for the mass flux (equation (14)). A

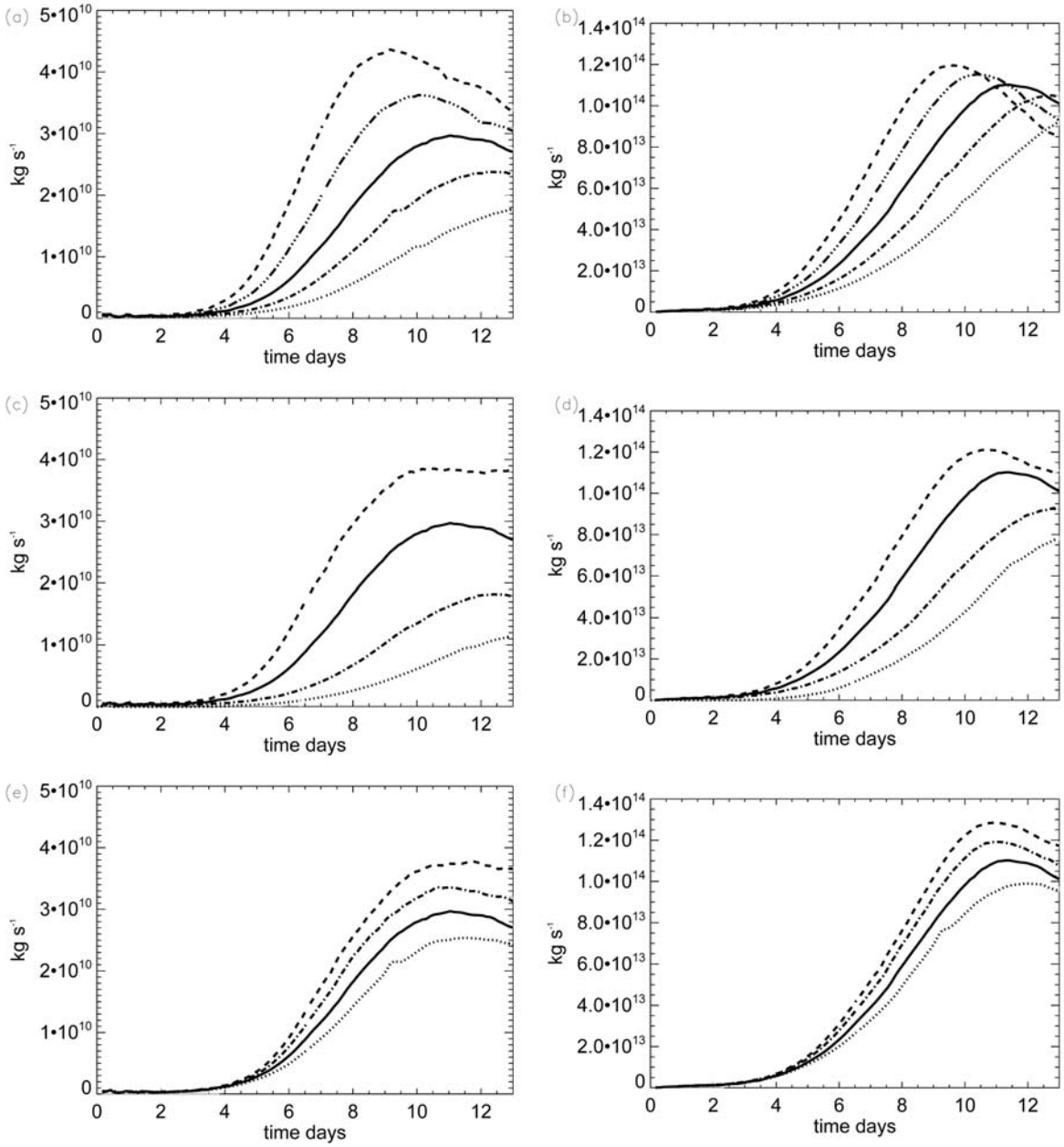

Figure 7. (left) Domain-integrated mass flux and (right) tracer flux for (a, b) different jet strengths: dotted line, 35 m s^{-1}; dash-dotted line, 40 m s^{-1}; solid line, 45 m s^{-1}; dash-dot-dotted line, 50 m s^{-1}; and dashed line, 55 m s^{-1}. (c, d) Different tropospheric stratifications: dotted line, $\partial\theta/\partial z$ = 0.008 K m^{-1}; dash-dotted line, $\partial\theta/\partial z$ = 0.006 K m^{-1}; solid line, $\partial\theta/\partial z$ = 0.004 K m^{-1}; and dashed line, $\partial\theta/\partial z$ = 0.003 K m^{-1}. (e, f) Different latitudes of the jet's center: dashed line, 40°N; solid line, 45°N; dash-dotted line, 50°N; and dashed line, 55°N.

very strong correlation can be seen. This proves that the large-scale dynamics exert a strong control on the rate of ventilation of mass. The exact magnitudes of the actual mass flux and the estimated fluxes are not the same. This is due to the values used for V_g in equation (7), the maximum zonal jet value. It would be more appropriate to take a low-level wind speed, which is responsible for the thermal advection that results in the warm conveyor belt ascent. When this method is used, a direct 1:1 correction is found (not shown). However, this method requires the use of data from each life cycle (e.g., the mean southerly wind component in the warm sector at a given level) and therefore is less useful in a climatological sense and would prevent equation (14) from being used to predict the amount of ventilation in future climates.

[42] The total amount of mass ventilated over the duration of the life cycles can also be compared to the mass flux diagnostic. To estimate the total ventilation equation (14) is multiplied by the time that ventilation occurs over, taken to be 10 days (no significant ventilation was observed between day 0 and day 3). This correlation is plotted in Figure 8b. Again, a strong linear correlation is found to exist between

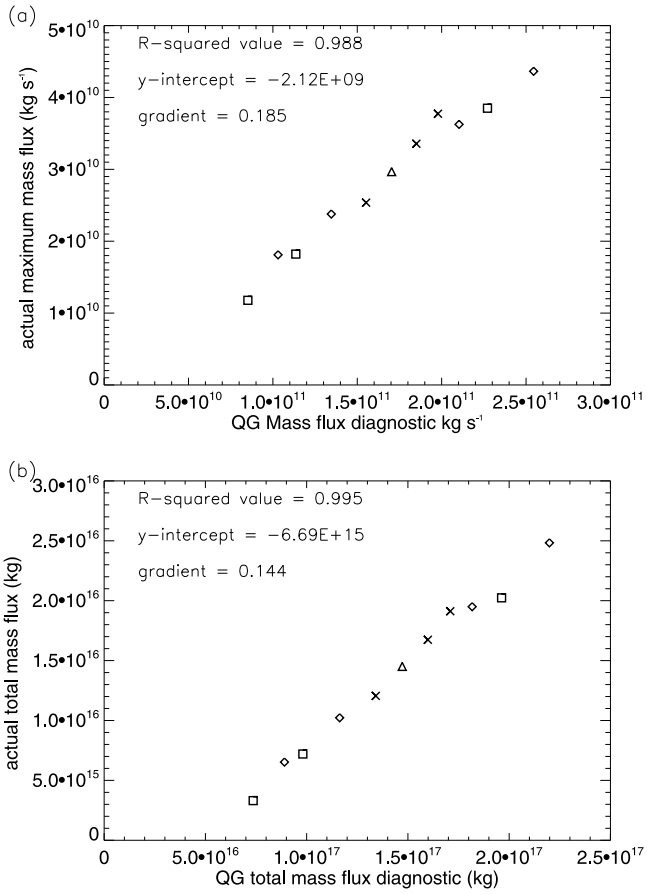

Figure 8. (a) Maximum domain-integrated instantaneous mass flux against the mass flux diagnostic for all experiments with different values of jet strength (diamonds), jet latitude (crosses), and tropospheric stability (squares). The triangle is the control simulation. (b) Total mass ventilated against the diagnostic for total mass flux. Symbols have same meanings as for Figure 8a.

the mass flux diagnostic and the total amount of ventilation. To quantify the relationships shown in Figure 8 the R^2 values, y intercept values, and the gradients of the best fit lines that could be fitted to the data are also shown in Figure 8. Both linear regressions have strongly positive gradients demonstrating that as the system's strength increases, the amount of ventilation does so as well.

[43] In order to develop a similar diagnostic for the tracer flux, an estimate of the tracer concentration at the top of the boundary layer is required (the tracer flux is the product of the mass flux and the tracer concentration). It is not possible to obtain values of tracer concentration from a scale analysis, and hence, we do not compare the actual tracer fluxes to a tracer flux diagnostic. However, the mass flux diagnostic can be considered as the uppermost bound on the tracer flux, hence allowing the maximum possible tracer ventilation to be estimated.

7. Conclusions

[44] The aim of this research was to investigate the relative importance of the transport processes identified by *Sinclair et al.* [2008] (horizontal convergence within the boundary layer and large-scale advection by the warm conveyor belt) and to identify which process controls the amount of boundary layer ventilation. This was achieved by simulating a number of idealized baroclinic life cycles using the idealized version of the Met Office Unified Model. Two sets of experiments were conducted, one to quantify the importance of the boundary layer transport processes and one to quantify the importance of the large-scale dynamics.

[45] The results have shown that the amount of boundary layer ventilation is controlled by the large-scale dynamics, and therefore, the strength of the warm conveyor belt acts as the rate limiting step in determining the amount of ventilation. This can be concluded by the strong linear correlation that was found between the mass flux diagnostic and both the maximum rate of ventilation and the total amount of ventilation out of the boundary layer. In direct contrast, the surface drag, and hence the horizontal convergence and divergence within the boundary layer, was found to have little impact on the amount of boundary layer ventilation when realistic values of surface drag were used. Only during the later stages of the smooth and no drag life cycles was the importance of the horizontal transport of tracer within the boundary layer realized. With little drag the horizontal convergence of tracer into the warm conveyor belt source region was weaker than the removal of tracer due to the warm conveyor belt's ascent, and therefore, in this unphysical parameter space, the rate-limiting step is the horizontal divergence and convergence within the boundary layer. However, for realistic values of surface drag, the horizontal transport within the boundary layer is not a limiting step on the efficiency of cyclones to ventilate the boundary layer.

[46] This demonstrates that from a theoretical viewpoint two possible ventilation regimes exist: one over rough (realistic) surfaces in which the large-scale dynamics limit the amount of ventilation and the second over very smooth (unrealistic) surfaces where boundary layer transport processes limit the amount of ventilation. However, the second regime does not occur within realistic parameter space and therefore would not be observed in any ventilation case studies.

[47] These results have considerable consequences for climatology studies. The large-scale dynamical variables that are required to estimate the mass flux diagnostic are available in reanalysis data sets, such as ERA-40, and in smaller cyclone databases. Therefore, climatologies of boundary layer ventilation could be derived by estimating the mass flux diagnostic for each cyclone in different storm tracks and therefore obtaining an estimate of the potential amount of ventilation. Additionally, in numerical simulations of the future climate, the location and strength of the midlatitude jet and the tropospheric stability may be examined to estimate how ventilation characteristics of midlatitude cyclones may change in the future. In such climatological studies it would not be necessary to treat cyclones over land differently to those over the ocean as the amount of ventilation was found to be independent of the magnitude of surface drag. This is would simplify the task of calculating a climatology considerably.

[48] **Acknowledgments.** The authors thank the Met Office for the use of their Unified Model. V. Sinclair was supported by NERC award NER/S/C/2005/13377.

References

Adamson, D. S., S. E. Belcher, B. J. Hoskins, and R. S. Plant (2006), Boundary-layer friction in midlatitude cyclones, *Q. J. R. Meteorol. Soc.*, *132*, 101–124.

Agustí-Panareda, A., S. Gray, and J. Methven (2005), Numerical modeling study of boundary-layer ventilation by a cold front over Europe, *J. Geophys. Res.*, *110*, D18304, doi:10.1029/2004JD005555.

Agustí-Panareda, A., S. L. Gray, and S. E. Belcher (2009), On the dependence of boundary layer ventilation on frontal type, *J. Geophys. Res.*, *114*, D05305, doi:10.1029/2008JD010694.

Arya, S. P. (1999), *Air Pollution Meteorology and Dispersion*, Oxford Univ. Press, New York.

Bethan, S., G. Vaughan, C. Gerbig, A. Volz-Thomas, H. Richer, and D. A. Tiddeman (1998), Chemical air mass differences near fronts, *J. Geophys. Res.*, *103*, 13,413–13,434.

Bey, I., D. J. Jacob, J. A. Logan, and R. M. Yantosca (2001), Asian chemical outflow to the Pacific in spring: Origins, pathways, and budgets, *J. Geophys. Res.*, *106*, 23,097–23,113.

Browning, K. A. (1985), Conceptual models of precipitating systems, *Meteorol. Mag.*, *114*, 293–319.

Carlson, T. N. (1980), Airflow through midlatitude cyclones and the comma cloud pattern, *Mon. Weather Rev.*, *108*, 1498–1509.

Davies, T., M. J. P. Cullen, A. J. Malcolm, M. H. Mawson, A. Staniforth, A. A. White, and N. Wood (2005), A new dynamical core for the Met Office's global and regional modelling of the atmosphere, *Q. J. R. Meteorol. Soc.*, *131*, 1759–1782.

Donnell, E., D. J. Fish, E. M. Dicks, and A. J. Thorpe (2001), Mechanisms for pollutant transport between the boundary layer and the free troposphere, *J. Geophys. Res.*, *106*, 7847–7856.

Eckhardt, S., A. Stohl, H. Wernli, P. James, C. Forster, and N. Spichtinger (2004), A 15-year climatology of warm conveyor belts, *J. Clim.*, *17*, 218–237.

Ekman, V. W. (1905), On the influence of the Earth's rotation on ocean currents, *Ark. Mat. Astron. Fys.*, *2*, 1–53.

Esler, J. G., P. H. Haynes, K. S. Law, H. Barjat, K. Dewey, J. Kent, S. Schmitgen, and N. Brough (2003), Transport and mixing between airmasses in cold frontal regions during Dynamics and Chemistry of Frontal Zones (DCFZ). *J. Geophys. Res.*, *108*(D4), 4142, doi:10.1029/2001JD001494.

Farrell, B. (1985), Transient growth of damped baroclinic waves, *J. Atmos. Sci.*, *42*, 2718–2727.

Haltiner, G. J., and R. T. Williams (1980), *Numerical Prediction and Dynamic Meteorology*, 2nd ed., John Wiley, New York.

Hannan, J. R., H. E. Fuelberg, J. H. Crawford, J. L. Sachse, and D. R. Blake (2003), Role of wave cyclones in transporting boundary layer air to the free troposphere during the spring 2001 NASA/TRACE-P experiment, *J. Geophys. Res.*, *108*(D20), 8785, doi:10.1029/2002JD003105.

Harrold, T. W. (1973), Mechanisms influencing the distribution of precipitation within baroclinic disturbances, *Q. J. R. Meteorol. Soc.*, *99*, 232–251.

Hess, P. G. (2005), A comparison of two paradigms: The relative global roles of moist convective versus non-convective transport, *J. Geophys. Res.*, *110*, D20302, doi:10.1029/2004JD005456.

Hess, P. G., and T. Vukicevic (2003), Intercontinental transport, chemical transformations, and baroclinic systems, *J. Geophys. Res.*, *108*(D12), 4354, doi:10.1029/2002JD002798.

Hines, K. M., and C. R. Mechoso (1993), Influence of surface drag on the evolution of fronts, *Mon. Weather Rev.*, *121*, 1152–1175.

Holton, J. R. (1992), *An Introduction to Dynamical Meteorology*, Academic, San Diego, Calif.

Holtslag, A. A. M., and B. A. Boville (1993), Local versus nonlocal boundary layer diffusion in a global climate model, *J. Clim.*, *6*, 1825–1842.

Hoskins, B., M. Pedder, and D. W. Jones (2003) The omega equation and potential vorticity, *Q. J. R. Meteorol. Soc.*, *129*, 3277–3303.

Kowol-Santen, J., M. Beekman, S. Schmitgen, and K. Dewey (2001), Tracer analysis of transport from the boundary layer to the free troposphere, *Geophys. Res. Lett.*, *28*, 2907–2910.

Lock, A. P., A. R. Brown, M. R. Bush, G. M. Martin, and R. N. B. Smith (2000), A new boundary layer mixing scheme. Part 1: Scheme description and single-column model tests, *Mon. Weather Rev.*, *128*, 3187–3199.

Polvani, L. M., and J. G. Esler (2007), Transport and mixing of chemical airmasses in idealized baroclinic lifecycles, *J. Geophys. Res.*, *112*, D23102, doi:10.1029/2007JD008555.

Roe, P. L. (1986), Characteristic-based schemes for the Euler equations, *Annu. Rev. Fluid Mech.*, *18*, 337–365.

Rotunno, R., and J. W. Bao (1996), A case study of cyclogenesis using a model hierarchy, *Mon. Weather Rev.*, *124*, 1051–1066.

Shapiro, M. A., and D. A. Keyser (1990), Fronts, jet streams, and the tropopause, in *Extratropical Cyclones: The Erik Palmén Memorial Volume*, edited by C. W. Newton and E. O. Holopainen, pp. 167–191, Am. Meteorol. Soc., Boston, Mass.

Simmons, A. J., and B. J. Hoskins (1978), The lifecycles of some nonlinear baroclinic waves, *J. Atmos. Sci.*, *35*, 414–432.

Sinclair, V. A., S. L. Gray, and S. E. Belcher (2008), Boundary-layer ventilation by baroclinic life cycles, *Q. J. R. Meteorol. Soc.*, *134*, 1409–1424.

Sinclair, V. A., S. E. Belcher, and S. L. Gray (2009), Synoptic controls on boundary-layer structure, *Boundary Layer Meteorol.*, doi:10.1007/s10546-009-9455-6.

Stull, R. B. (1988), *An Introduction to Boundary Layer Meteorology*, 1st ed., Kluwer Acad., Dordrecht, Netherlands.

Troen, I. B., and L. Mahrt (1986), A simple model of the atmospheric boundary layer; Sensitivity to surface evaporation, *Boundary Layer Meteorol.*, *37*, 129–148.

Williams, G. P., and J. B. Robinson (1974), Generalized Eady waves with Ekman pumping, *J. Atmos. Sci.*, *31*, 1768–1776.

S. E. Belcher and S. L. Gray, Department of Meteorology, University of Reading, Earley Gate, PO Box 243, Reading RG6 6BB, UK.

V. A. Sinclair, Division of Atmospheric Sciences and Geophysics, Department of Physics, University of Helsinki, Erik Palmenin Aukio 1, FI-00560 Helsinki, Finland. (victoria.sinclair@helsinki.fi)